

Effect of geometry on droplet formation in the squeezing regime in a microfluidic T-junction

Amit Gupta · Ranganathan Kumar

Received: 29 July 2009 / Accepted: 28 September 2009 / Published online: 15 October 2009
Springer-Verlag 2009

Abstract In the surface tension-dominated microchannel T-junction, droplets can be formed as a result of the mixing of two dissimilar, immiscible fluids. This article presents results for very low Capillary numbers and different flow rates of the continuous and dispersed phases. Through three-dimensional lattice Boltzmann-based simulations, the mechanism of the formation of “plugs” in the squeezing regime has been examined and the size of the droplets quantified. Results for $Re_c \ll 1$ show the dependence of flow rates of the two fluids on the length of the droplets formed, which is compared with existing experimental data. It is shown that the size of plugs formed decreases as the Capillary number increases in the squeezing regime. This article clearly shows that the geometry effect, i.e., the widths of the two channels and the depth of the assembly, plays an important role in the determination of the length of the plugs, a fact that was ignored in earlier experimental correlations.

Keywords Microfluidics · Capillary number · Lattice Boltzmann · Multiphase flow

List of symbols

a Acceleration
 a Index for velocity-space discretization

A. Gupta
Department of Aerospace Engineering, University of Michigan,
Ann Arbor, MI 48109, USA
e-mail: amitgupt@umich.edu

R. Kumar (✉)
Department of Mechanical, Materials and Aerospace
Engineering, University of Central Florida, Orlando,
FL 32816, USA
e-mail: Rnkumar@mail.ucf.edu

Dimensionless length of the emerging droplet
Lattice unit length
Color field
Capillary number = $\mu_c U / \sigma$
Speed of sound
Diameter of the drop
Lattice speed of particles moving in direction
Particle distribution function
Force
Unit tensor
Droplet length
Normal vector at the interface
Number of links at each lattice point
Pressure
Momentum
Flow rate/ratio
Radius of the drop
Reynolds number = UD/ν
Time
Velocity
Droplet volume
Width of the channel/weight along link

Greek symbols

β Parameter controlling the width of the interface
 γ Lattice weights
 $\delta_{\alpha\beta}$ Kronecker delta
 κ Curvature
 λ Viscosity ratio
 ρ Density
 σ Surface tension
 μ Dynamic viscosity
 ν Kinematic viscosity
 τ Relaxation time
 φ Angle

∇	Gradient
Γ	Height-to-width ratio
Λ	Dispersed-to-continuous channel width ratio
Ω	Collision operator

Subscripts

B	Blue fluid
c	Continuous phase
d	Dispersed phase
eff	Effective
ext	External
growth	Growth
i	Index
in	Inside the drop
out	Outside the drop
R	Red fluid
Spur	Spurious
x	x-component
y	y-component

Superscripts

*	Non-dimensional quantities
eq	Equilibrium

1 Introduction

In recent years, microfluidic devices that generate emulsions of liquid droplets suspended in an outer immiscible liquid have found widespread applications in food processing, drug delivery, microanalysis, tumor destruction, ultrasound agents and in chemical reactions at the microscale level (Christopher et al. 2007). Many applications are found that involve multiphase transport through thin capillaries and microchannels. For instance, miniature evaporative and distillation units and bubble generators, flow cytometers and emulsions all use transport of two dissimilar fluids through a microchannel. Over the past few years, numerous experiments have highlighted the advantages of microfluidic devices, particularly using co-flowing fluids (Umbanhowar et al. 2000; Cramer et al. 2004), passing dissimilar fluids through an orifice (Anna et al. 2003; Garstecki 2005) and droplet formation at T-junctions (Thorsen et al. 2001; Garstecki et al. 2006; Van der Graaf et al. 2006; Tice et al. 2004; Guillot and Colin 2005; Husny and Cooper-White 2006; Christopher et al. 2008; Gupta et al. 2009; De Menech et al. 2008). Due to the length scales involved, the flow of the dissimilar fluids falls in the laminar regime, which enables a higher degree of control on the injection process (Christopher et al. 2007). The large surface-to-volume ratio enhances the role of surface tension effects. The experimental data (Guillot and Colin 2005) show that when for a given continuous phase flow rate, if the dispersed flow is increased, the flow pattern changes from droplets at T-junction to droplets in channel. This indicates that for a given Capillary number $Ca = \mu_c U_d / \sigma$, when the flow rate ratio $Q = Q_d / Q_c$ is increased, a regime change occurs. With further increase in the flow rate, the flow regime changes to parallel flow. While these transitions may not occur until the flow rate ratio becomes large for low Ca, they occur earlier for high Ca (Gupta et al. 2009). The physical laws could be derived mainly on the basis of an understanding of multiphase flows and controlling the fluid streams in microchannels. The other physical variables that influence droplet formation in microchannels are the flow rates of the continuous and dispersed phases, viscosities of the fluids, geometry of the device, and interplay of surface tension and viscous forces.

Although experimental (Thorsen et al. 2001; Garstecki et al. 2006; Tice et al. 2004; Guillot and Colin 2005; Husny and Cooper-White 2006; Christopher et al. 2008) and numerical (Van der Graaf et al. 2006; Gupta et al. 2009; De Menech et al. 2008) studies on the formation of droplets at a T-junction have caught the attention of the practicing engineer, a fundamental understanding of the flow physics that could account for the effect of the geometry of the flow device is missing. In addition, simulations of multiphase flows in complex flow geometries are a challenging class of problems. In this study, the lattice Boltzmann method (LBM) has been used to simulate two-fluid flows for the formation of droplets past a T-junction microfluidic device. In recent years, LBM has emerged as a powerful tool for many applications involving complex fluid flow, in particular, in the formation of a secondary or disperse flow. LBM starts from meso- and microscopic Boltzmann's kinetic equation and can be used to determine macroscopic fluid dynamics. The objective of this study is to simulate and classify the formation of droplets in T-junction microfluidic flows for situations where the detachment of the dispersed phase is influenced by the strength of surface tension forces mitigated between the dissimilar fluids. In addition, no theoretical study that has investigated the effect of the geometry of the microfluidic device on the size and shape of the droplets collected downstream at the outlet exists. Through numerical simulations, we have reported the role of the geometric parameters in the framework of this statistical method.

2 Methodology

LBM can be regarded to be a finite-difference formulation for the kinetic equation of the particle distribution function f_i along the direction \vec{e}_i (Chen and Doolen 1998), and is

$$f_i(x + e_i \delta t, t + \delta t) = f_i(x, t) + \Omega_i(f_i(x, t)),$$

$$i = 0, 1, \dots, N,$$

where $\Omega_i(f_i(x, t)) = -\frac{f_i(x, t) - f_i^{eq}(x, t)}{\tau}$ (1)

Ω_i is the linearized collision operator with the single relaxation time approximation, and is commonly known as the lattice BGK (Bhatnagar-Gross-Krook) operator. f_i^{eq} and τ are the local equilibrium distribution and the dimensionless relaxation time, respectively. The macroscopic density and momentum flux can be obtained from the distribution functions given by

$$\rho = \sum_i f_i = \sum_i f_i^{eq}, \quad \rho u = \sum_i f_i e_i = \sum_i f_i^{eq} e_i$$
 (2)

where

$$f_i^{eq} = \gamma_i \rho \left[1 + 3e_i \cdot u + \frac{9}{2}(e_i \cdot u)^2 - \frac{3}{2}u \cdot u \right]$$
 (3)

and for the D3Q19 lattice used in this study, the weights are given as

$$\gamma_i = \begin{cases} 1/3 & \text{for } i = 0 \\ 1/18 & \text{for } i = 1, \dots, 6 \\ 1/36 & \text{for } i = 7, \dots, 18 \end{cases}$$
 (4)

Chen and Doolen (1998) have shown that Eq. 1 can be reduced to the Navier-Stokes equations in the low frequency, long wavelength limit using the Chapman-Enskog expansion together with Eq. 2. As a result, the pressure and viscosity are written as $p = c_s^2 \rho$ and $\nu = (\tau - 1/2)c_s^2 \delta t$.

Numerous methods have been used by researchers over the last decade to conduct multiphase simulations using LBM. These include the chromodynamic (Gunstensen et al. 1991), pseudo-potential (Shan and Chen 1993), free-energy (Swift et al. 1995), and the projection (Inamuro et al. 2004) methods. Each of these formulations has its own advantages and disadvantages. The chromodynamic and pseudo-potential methods are widely used to simulate multiphase flows because of their ease of implementation and isotropic nature of solutions. However, (a) velocity vectors are high at the interface, (b) momentum is not conserved locally, and (c) the models work well for low density ratios only. On the contrary, in the free-energy approach local momentum conservation was satisfied, although the model suffers from the lack of Galilean invariance. In a recent and robust scheme for the treatment of the interface (Lishchuk et al. 2003), a two-fluid mixture is kept separated through a diffuse interface that spans a few lattice nodes. The location of the interface is controlled by a surface tension force which is incorporated such that

the stress boundary condition and the continuity of velocity across the interfacial line are satisfied. The model has several advantages over earlier formulations, which include low spurious currents, relatively thin interface, treatment of up to three species, and non-iterative computations. The disadvantage of the model is that it can only handle fluids with similar densities. This model begins with the elementary two-phase method of Gunstensen et al. (1991). In the original method (Gunstensen et al. 1991), two particle distributions denote the two different fluids. Each fluid is assigned a color (the use of the word color is meant for identifying the fluid only) at all the locations in the domain of interest. Each of these colored phases undergoes the collision and streaming operations, given as

$$f_i^{k,AC}(x, t) = f_i^k(x, t) - \frac{f_i^k(x, t) - f_i^{k,eq}(x, t)}{\tau_k} + \Phi_i$$
 (5)

where k denotes the Red or Blue distribution and $f_i^{k,AC}$ denotes the post-collision quantity. The kinematic viscosity of each fluid can be written as $\nu = c_s^2(\tau_k - 1/2)$, where $k = R$ or B . Moreover, the densities of each of the phases is given by

$$\rho_R = \sum_i f_i^R(x, t)$$
 (6a)

$$\rho_B = \sum_i f_i^B(x, t)$$
 (6b)

In addition to a collision operation given by the above mentioned equation, the particle distributions undergo a second collision (also known as the perturbation step),

$$f_i^k(x + e_i, t + 1) = f_i^{k,AC}(x, t) + A|G| \cos 2(\theta_i - \theta_f)$$
 (7)

where A is a parameter related to the interfacial tension, θ_i is the polar angle of the lattice direction, and θ_f is the polar angle of the local color gradient, which is calculated as

$$G(x, t) = \sum_i \gamma_i e_i (\rho_R(x + e_i, t) - \rho_B(x + e_i, t))$$
 (8)

In order to prevent the numerical diffusion of the two fluids across the interface, a re-coloring step is required, which enables to keep the interface sharp, and at the same time prevents mixing of the two fluids at the interface. The colored distributions are de-mixed by maximization of the work done by the color flux.

$$g(x, t) = \sum_i \gamma_i e_i (f_i^R(x, t) - f_i^B(x, t))$$
 (9)

The original model carries certain disadvantages which crucially underpins its applicability to study low Reynolds number flows. First, the re-coloring step is known to introduce lattice pinning, a phenomenon in which the interface can be stuck at a lattice node and is unable to conform to the physical motion of the dynamic interface,

rendering the simulation ineffective. Second, the perturbation step has the side effect of introducing anisotropy and high spurious velocities at the interface (Lishchuk et al. 2003; Wu et al. 2008).

The recent improvement (Lishchuk et al. 2003) modified the original model to relieve the method of the perturbation step. Subsequently, this step was replaced with a direct forcing term at the sites where mixing of the two phases occurs. In order to impose the stress boundary condition and the continuity equation for the incompressible fluids, the model (Lishchuk et al. 2003) introduced a local pressure gradient throughout the interface, which is incorporated into the collision step. This force is defined such that it acts normal to the interface, centripetally and with a magnitude that is proportional to the gradient of the phase field, defined as

$$\rho^N(x, t) = \frac{\rho^R(x, t) - \rho^B(x, t)}{\rho^R(x, t) + \rho^B(x, t)} \quad (10)$$

Clearly, $-1 \leq \rho^N(x, t) \leq 1$. The local curvature at the mixed locations on the interface is computed based on the normal vector computed at the particular lattice location. The normal vector, is defined as a function of the phase field, and is given by

$$n = -\frac{\nabla \rho^N}{|\nabla \rho^N|} \quad (11)$$

Based on the local normal vector, the radius of curvature, R , of the interface is computed as

$$\kappa = \frac{1}{R} = -\nabla_s \cdot n \quad (12)$$

where κ is the curvature and

$$\nabla_s = (I - nn) \cdot \nabla \quad (13)$$

where I is the unit tensor and ∇_s is the surface gradient operator.

Based on the curvature, the source term is calculated such that it incorporates the surface tension force, and is given as

$$\Phi_i = \frac{\gamma_i}{c_s^2} F \cdot e_i \quad (14)$$

where

$$F(x, t) = \frac{1}{2R} \sigma \nabla \rho^N \quad (15)$$

The partial derivatives of the components of the normal vector are computed based on a formulation for discretizing a general function ϕ on a regular lattice with contributions from the neighboring lattice sides,

$$\frac{\partial \phi}{\partial x} = \frac{1}{c_s^2} \sum_i \phi(x + e_i) e_{ix} \gamma_i \quad (16a)$$

and

$$\frac{\partial \phi}{\partial y} = \frac{1}{c_s^2} \sum_i \phi(x + e_i) e_{iy} \gamma_i \quad (16b)$$

In addition, the color segregation step of the original model (Gunstensen et al. 1991) was replaced by a recent variant (Latva-Kokko and Rothman 2005), which minimizes the spurious velocities even further, and at the same time removes lattice pinning. According to this method, the post-collision distributions of the two color fluids, red and blue, are computed as

$$f_i^R = \frac{\rho_R}{\rho_R + \rho_B} f_i + \gamma_i \beta \frac{\rho_R \rho_B}{(\rho_R + \rho_B)} \cos \theta_f |e_i| \quad (17a)$$

$$f_i^B = \frac{\rho_B}{\rho_R + \rho_B} f_i - \gamma_i \beta \frac{\rho_R \rho_B}{(\rho_R + \rho_B)} \cos \theta_f |e_i| \quad (17b)$$

where

$$\cos \theta_f = \frac{e_i \cdot \nabla \rho^N}{|e_i| |\nabla \rho^N|} \quad (18)$$

β is the anti-diffusion parameter and is fixed at 0.7 to keep the spurious currents low and maintain a narrow interface thickness (Lishchuk et al. 2008).

3 Results and discussion

Before beginning large scale three-dimensional multiphase simulations, the accuracy of the model selected (Lishchuk et al. 2003; Latva-Kokko and Rothman 2005) was established by conducting the static bubble test in a two-dimensional 101×101 periodic domain for different initial diameters. The difference in the pressure inside and outside the bubble is given as a function of the interfacial tension and radius by the Laplace's law,

$$p_{in} - p_{out} = \Delta p = \frac{\sigma}{R} \quad (19)$$

Simulations were conducted for different sizes of the bubble for a fixed interfacial tension parameter to compare the pressure difference at equilibrium with that prescribed by the Laplace's law, and the results are shown in Fig. 1. A linear dependence between Δp versus $1/R$ indicates that the current model correctly incorporates the stress boundary condition at the two-fluid interface. The validation was verified for viscosity ratios of 1 and 10 to confirm the viscosity-independent nature for comparison with Laplace's law. The same pressure versus inverse radius dependence was observed for this wide range of viscosities. Lishchuk et al. 2003 have shown that for radii greater than two lattice units, the initial prescribed surface tension can be expected to be close to within 5–10% of the macroscopic surface tension as dictated by the Laplace's law, which was observed in this study as well.

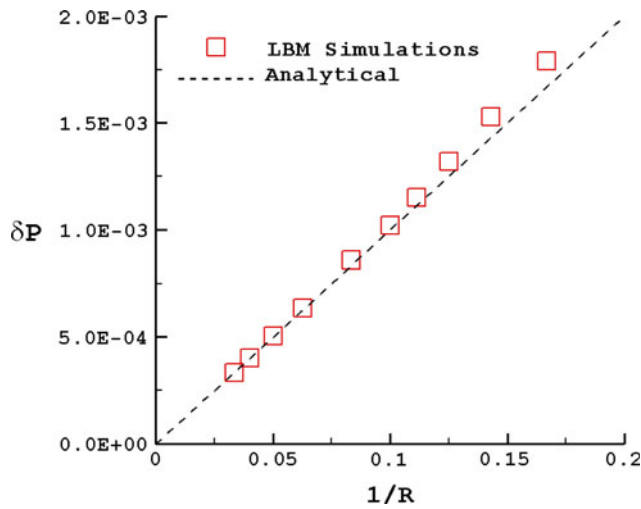


Fig. 1 Difference in the inside and outside pressure for the static bubble test with $\sigma = 0.01$ for different size bubbles. The linear variation denotes a constant value of the interfacial tension parameter

Simulation results for the formation of droplets in a T-junction device are reported next. The important parameters that can influence the droplet formation process can be written in terms of the physical parameters that define the two-fluid flow. The three-dimensional geometry of the T-junction is shown in Fig. 2, where the top and side views depict the channel dimensions and the flow inlets for the continuous and dispersed phase to enter. No-slip boundary conditions were employed using half-way bounceback schemes for the walls (Chen and Doolen 1998). At the inlet and outlet, mass flux was specified at each time step using $f_i^{eq}(\rho, u)$, in addition to a constant outlet pressure enforced

at the exit of the channel (Wu et al. 2008). It is assumed, for simplicity, that the two liquids have similar densities, which are given by ρ . Accordingly, the problem can be described in terms of the following dimensional and physical parameters: $w_c, w_d, h, U_c, U_d, \mu_c, \mu_d, \sigma$ and ρ . Based on these nine parameters, we can define six independent dimensionless parameters, using the Buckingham Pi theorem (De Menech et al. 2008). Selecting w_c, μ_c , and U_c as the primary dimensions, the volume of the droplets that are formed can be written as a function of the following six dimensionless groups:

$$\bar{V} = f(Q, \lambda, \Lambda, \Gamma, Ca, Re) \tag{20}$$

where $Q = \frac{U_d w_d h}{U_c w_c h} = \frac{U_d w_d}{U_c w_c}$, $Ca = \frac{\mu_c U_c}{\sigma}$, $Re = \frac{\rho U_c w_c}{\mu_c}$, $\lambda = \frac{\mu_d}{\mu_c}$, $\Gamma = \frac{h}{w_c}$ and $\Lambda = \frac{w_d}{w_c}$.

De Menech et al. (2008) argue that for low Reynolds number flows and $w_c = w_d = h$, the number of parameters reduce to Q, Ca , and λ . It is easy to establish that the Capillary number (Ca), which is a ratio of the viscous to the surface tension forces, is the most important parameter in flow situations where the two forces can affect simultaneously. In addition, as the droplet formation process in microchannels is highly laminar in nature, the characteristic velocity of the flow would inherently be small. In such a case, a model that can successfully simulate two dissimilar fluids, and at the same time achieve numerical stability at low velocities is highly desirable. Earlier simulations of LBM-based multiphase flows have adopted the pseudo-potential model (Shan and Chen 1993) to simulate drag behavior of multiple bubbles in infinite liquids (Gupta and Kumar 2008) or the projection method to simulate impingement of droplets on dry surfaces for high density ratios (Gu et al. 2009). Figure 3 represents a benchmark case to illustrate the spurious velocities on the surface of a two-dimensional (equilibrated) static drop. Two different simulations for equilibrating a static droplet were run, with the same initial diameter, such that the surrounding medium density is nearly the same as the liquid drop density. For the sake of comparison, the same surface tension parameter was chosen for both models, and the results at equilibrium are shown. The Shan-Chen model uses an interaction parameter G_{ij} to enforce the segregation of two fluids at the interface. The strength of this parameter determines the interfacial tension coefficient. In order to compare the spurious velocities of the Lishchuk and Shan-Chen models, the value of the interaction parameter in the latter was varied using multiple simulations until the surface tension evaluated after equilibration of the static drop matched with the input of the former. It was found that the ratio of the magnitude of spurious velocity of the pseudo-potential method (Shan and Chen 1993) to that of Lishchuk's model (Lishchuk et al. 2003) was of the order of 10,000. Moreover, the magnitude of spurious currents in

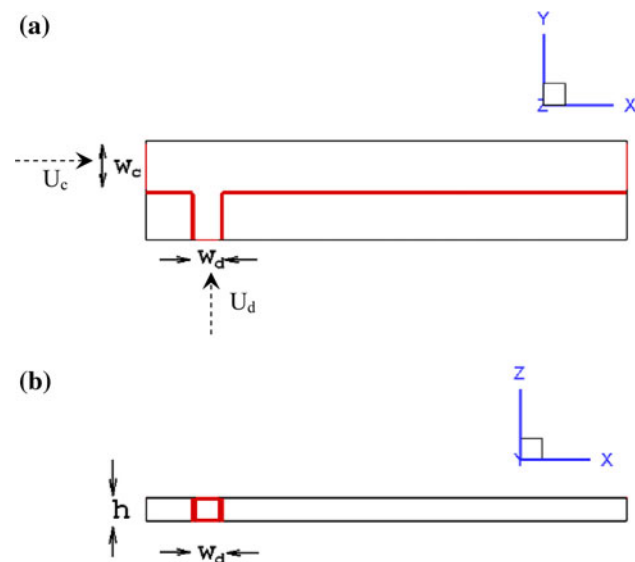
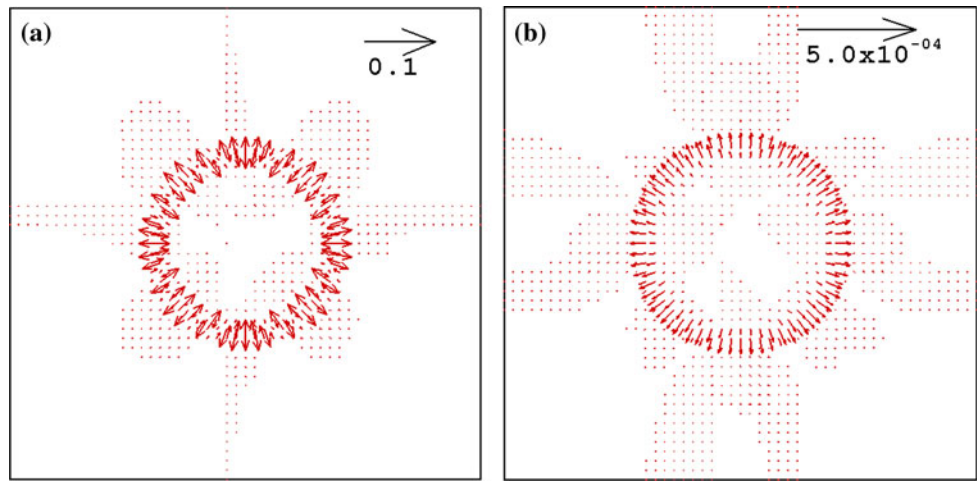


Fig. 2 a Top and b side view of the T-junction microchannel used for modeling formation of droplets. The inlet channels are marked using velocities at the appropriate faces

Fig. 3 Comparison of the spurious velocities at the interface of the two fluids with $\sigma = 0.01$ for a Shan-Chen model (1993) and b Lishchuk et al. (2003) using 2D simulations of a static droplet. The reference vectors for the spurious velocities are shown for visual guidelines only



terms of the droplet diameter and viscosities selected was $Re_{spur} = U_{spur} D / \nu = 3.6$ for Shan-Chen, whereas for Lishchuk's model it was $Re_{spur} = 0.001$, whereas the spurious Capillary numbers were 0.25 and 6.9×10^{-5} , respectively. Clearly, for the problem where the flow Reynolds number is of order 1, the Shan-Chen model does not offer a viable option, and thus was discarded, and simulation results using the Lishchuk's model are presented.

3.1 Droplet formation in the squeezing regime

The current model was verified by comparing the normalized droplet volume recorded using lattice Boltzmann simulations for $\Lambda = \Gamma = 1$ and $\lambda = 1/8$ for two flow rate ratios of $Q = 1/4$ and $1/8$ with the simulation results of De Menech et al. (2008). The mesh selected consisted of

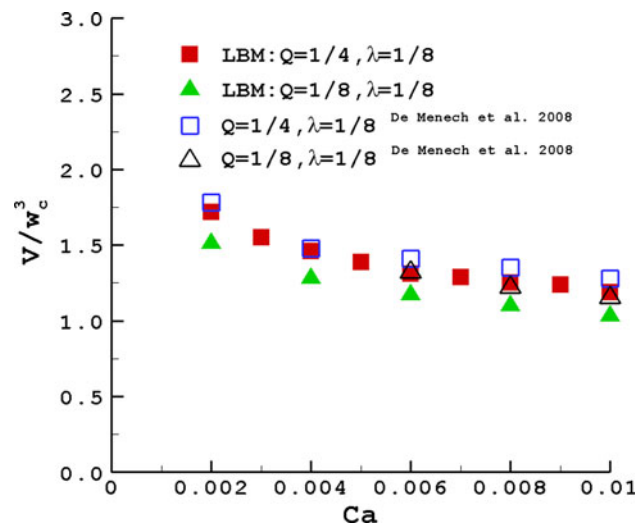


Fig. 4 Comparison of normalized volume from the current simulations with De Menech et al. (2008) for $\Lambda = 1$ and $\Gamma = 1$, viscosity ratio of $\lambda = 1/8$ and flow ratio $Q = 1/4$ and $1/8$

was $201 \times 21 \times 21$ nodes, and the comparison is shown in Fig. 4. It can be observed that the current simulation results are in agreement with the phase-field simulations (De Menech et al. 2008) with a maximum error of 7 and 10% for $Q = 1/4$ and $1/8$, respectively, where the maximum deviation is found to occur for the highest Ca simulated.

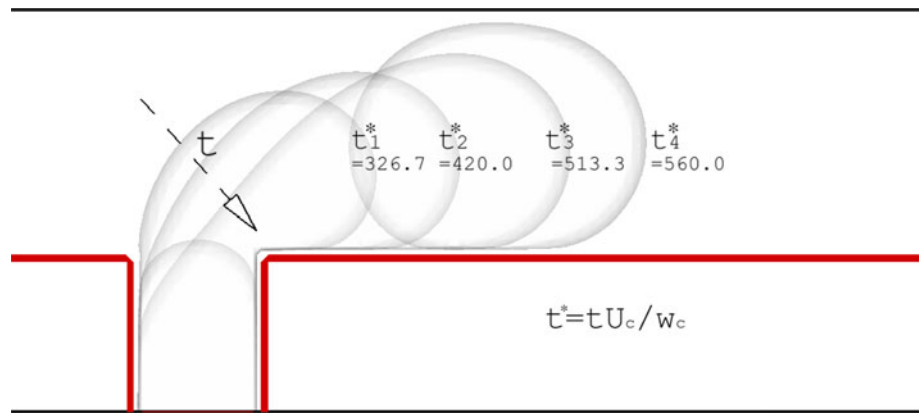
A time history of the movement of the two-fluid interface is shown in Fig. 5 for $Ca = 0.0028, Re_c = 0.22$, and $\Lambda = 1/2$, where the upstream interface is shown to be pushed down as the pressure of the liquid builds up due to a blockage of the available area for the continuous phase to flow. At low Capillary numbers ($Ca \ll 1$), droplet formation

is a direct consequence of the pressure force exerted by the continuous fluid on the dispersed phase. At such low Capillary numbers, the viscous drag force becomes negligible as compared to the surface tension forces that hold the interface together. In such a scenario, the viscous forces are not strong enough to overcome the interfacial force, and, hence, the droplet starts to grow in the main channel and block the flow of the continuous liquid, an observation consistent with earlier experiments (Garstecki et al. 2006).

The pressure gradient and the flow of continuous liquid aid in the distortion of the expanding droplet, due to which the interface progressively moves towards the exit of the main channel. Owing to the blockage of the available area for the continuous fluid to flow downstream, the pressure upstream of the expanding droplet increases, pushing the upstream interface toward the downstream edge of the junction. Eventually, the upstream interface is cut-off by the downstream edge of the dispersed phase channel, and a "plug" is formed. At this time, the interface retracts, and a new plug starts to penetrate the main channel.

Invariably, plugs formed by such a process are found to have a length that is of the same order as the width of the continuous phase channel. Moreover, the length depends on the flow rate of the dispersed phase at a fixed Capillary number of the continuous liquid. Figure 6 shows results for

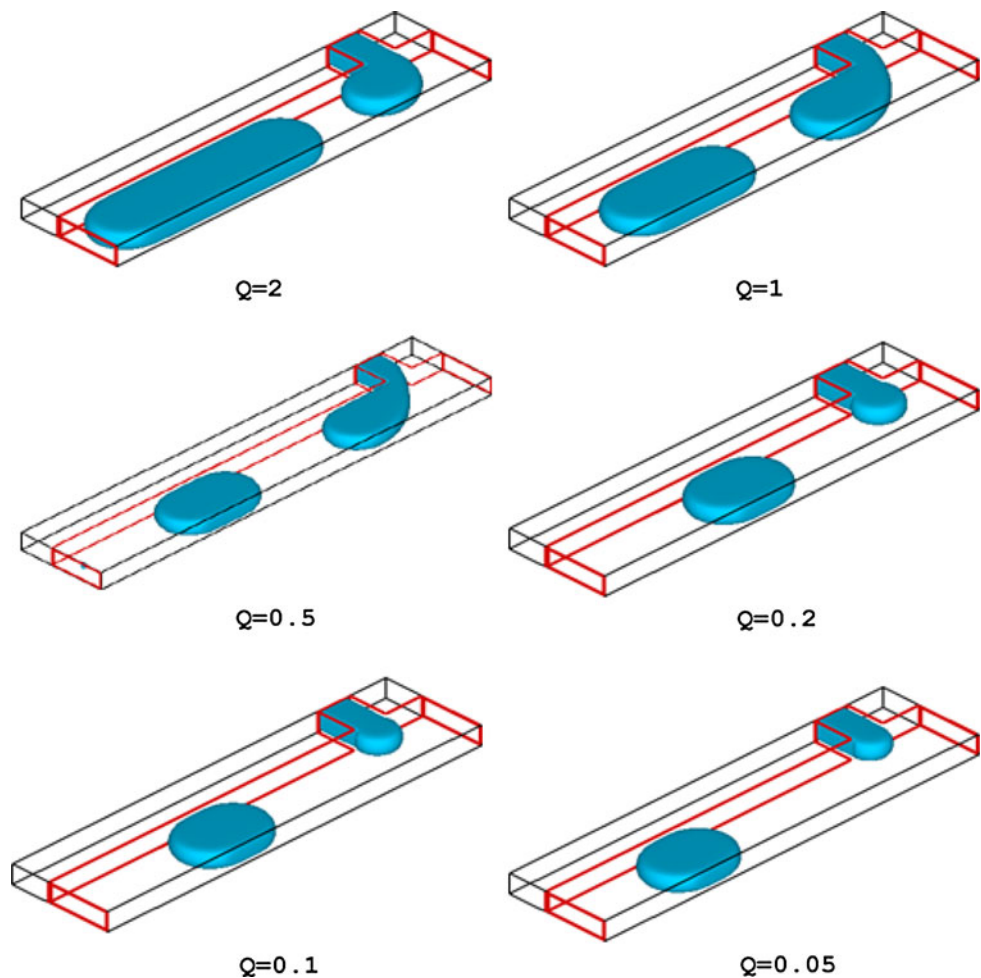
Fig. 5 Formation of a plug for $Ca = 0.0028$ and $\lambda = 1/2$ using lattice Boltzmann simulations. It can be observed that the upstream interface moves toward the downstream edge of the dispersed phase channel with time, where the interface is pinched off, eventually



$Ca = 0.001$, $Re_c = 0.085$, and $\lambda = 1/30$ for a range of flow rate ratios Q . The number of lattice nodes chosen was $201 \times 51 \times 11$ and the other geometric parameters were fixed at $\Lambda = 0.5$ and $\Gamma = 0.3$. In order to check grid independence, for the condition $Ca = 0.001$, $Q = 1$, $\lambda = 1/30$ and $\Lambda = 1/2$, the original mesh of $201 \times 51 \times 11$ was further refined to $301 \times 77 \times 16$. In addition, the discretized (non-dimensional) Boltzmann's equation makes use of

of the lattice velocity, $c = \Delta x / \Delta t = 1$. Hence, a finer dimensionless droplet length changed from 2.39 to 2.44 between the original and the refined mesh. Thus, the refinement leads to a change of only 2% in the predictions, which is small enough to justify the use of a coarser mesh for the time-consuming computations which decreased by $\Omega(N^3)$. The flow rate ratio was varied by increasing the

Fig. 6 Variation in the droplet length as a function of flow rate ratio for $Ca = 0.001$, $Re_c = 0.085$, $\lambda = 1/30$, and $\Lambda = 1/2$, $\Gamma = 0.3$



inlet velocity of the dispersed liquid and keeping the flow rate of the continuous liquid fixed. The length of the plugs formed was the highest when $Q = Q_d/Q_c = 2$, and is seen to be much larger than the width of the continuous phase channel. As the flow ratio was decreased, plugs of reduced length were formed (Fig. 6). For $Q \leq 1/5$, the length of the plugs was not found to change appreciably. Clearly, the role of the flow rates of the two fluids is a determining factor in the size of the droplets formed at the T-junction. The results for $Ca = 0.0028$, $\lambda = 1/30$ and two different sets of geometries ($\Lambda = 1/2$ and $1/3$) are shown in Fig. 7. The comparison with two sets of channel geometries was done to highlight how different geometries may result in different droplet sizes, a phenomenon not illustrated in the experimental correlations. The number of lattice nodes for geometries ($\Lambda = 1/2$ and $\Lambda = 1/3$) were $201 \times 51 \times 11$ and $201 \times 51 \times 19$, respectively. For $\Lambda = 1/2$, the length of the plugs formed at $Ca = 0.001$ given in Fig. 6. As the Capillary number was increased based on the velocity of the continuous liquid stream (i.e. U_c), the decrease in the length of the dispersed phase to the main channel is inversely related to the flow rate ratio. Once the drop is formed at the T-junction, the time to squeeze-off the emergent phase reduces as it is inversely related to the flow rate of the

Fig. 7 Outcomes for $Ca = 0.0028$ and two different geometries, given by $\Lambda = 1/2$ ($Re_c = 0.085$) and $\Lambda = 1/3$ ($Re_c = 0.48$) shown as a function of the flow rate ratio

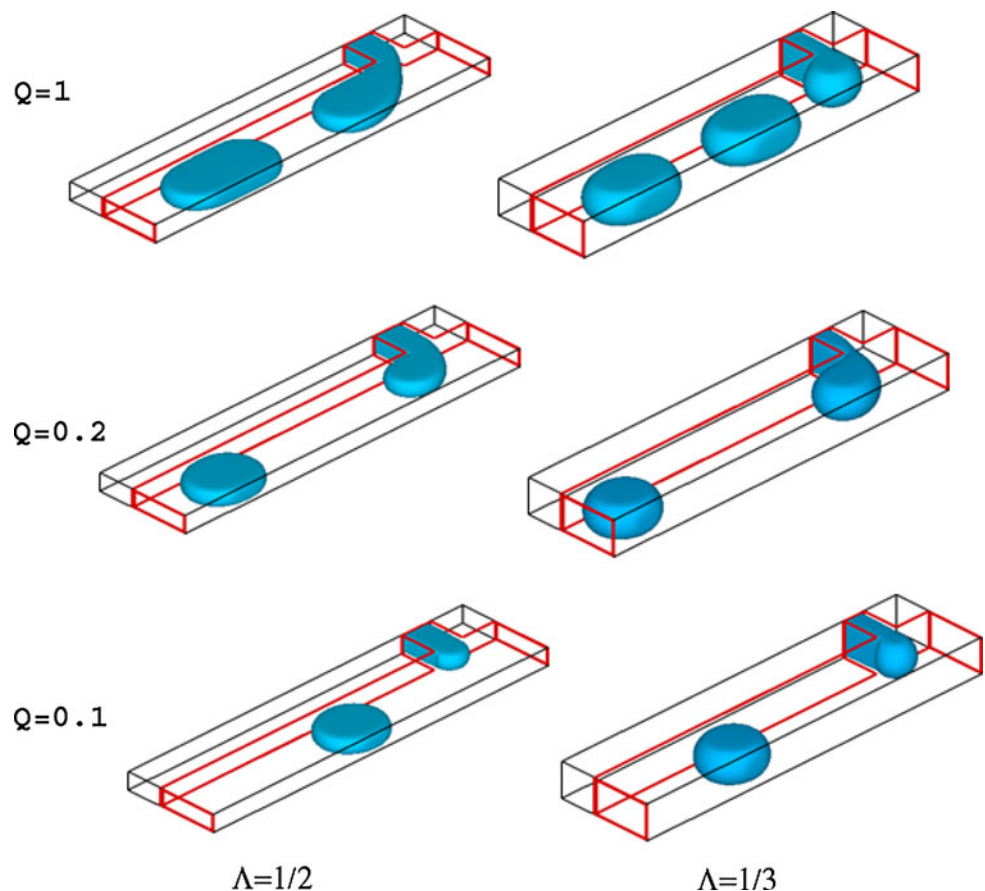
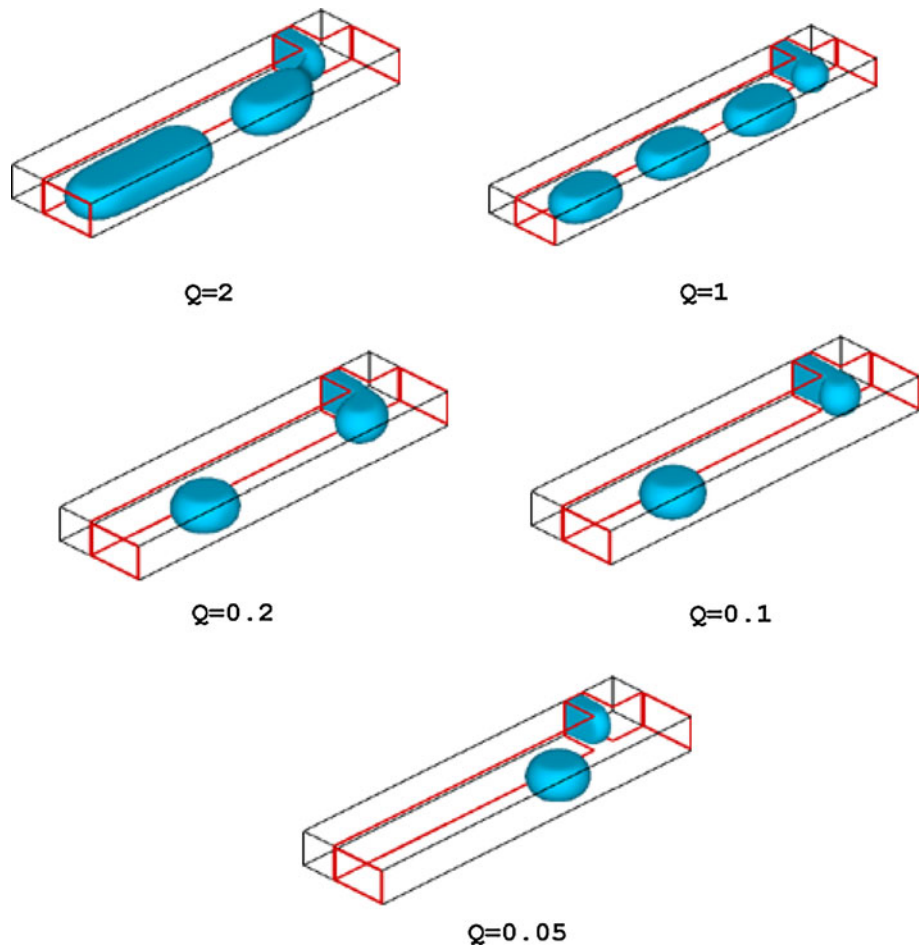


Fig. 8 Formation of plugs and cobbles as a function of flow rate ratio for $Ca = 0.006$, $Re_c = 0.13$, $\Lambda = 1/3$, $\Gamma = 0.6$, and $\lambda = 1/30$



continuous phase Q_c . Thus, below a certain flow rate ratio, $\alpha = d/w_c$ the emergent drop size would be independent of the flow rate ratio, and would seem to follow an asymptotic dependence. These are summarized in terms of the dimensionless length of droplets formed in this regime as a function of Q . Figure 9a and b show LBM data for two Capillary numbers for the geometric parameters $\Lambda = 1/2$ and $1/3$, respectively, whereas the normalized droplet volumes for the aforementioned cases is shown in Fig. 9c. In plots (a) and (b), the LBM data are compared with the correlations proposed by Garstecki et al. (2006) and Christopher et al. (2008). Neither of these correlations considered the geometry effects as is evident from the poor agreement of results in these figures. Garstecki et al. (2006) quantified the droplet sizes formed in a T-junction microfluidic channels for low Capillary number flows and for channels where $\Lambda = w_d/w_c$ lies between 0.25 and 1. Their experimental data indicates that the lengths of the drops formed at low Capillary numbers and for the range of channel widths given earlier can be written as

$$L/w_c = 1 + \alpha Q \tag{21}$$

where

(22) is a fitting parameter based on the characteristic width of the neck (\hat{d}_{neck}) and the flow rate ratio varied between 0.02 and 10. As the speed at which the neck collapses on the sharper downstream edge of the dispersed phase channel and the speed of the continuous fluid are not the same, the estimation of this fitting parameter becomes inherently difficult. Hence, this parameter was fitted to their experimental data and was found to be of order one. They also noted that the limiting case of droplet lengths correspond to $L \sim w_c$, suggesting that the continuous channel width plays a major role in the formation of the droplets. Although Eq. 21 was found to match well with their experimental results, the authors noticed that the applicability is questionable for channel geometries, where $\Lambda = w_d/w_c < 1/2$. A scaling mechanism has also been proposed recently (Christopher et al. 2008) by which the size of the droplets formed at a microfluidic T-junction can be estimated indirectly based on the Capillary number of the flow. According to this model, the formation of a droplet occurs when the interfacial force resisting the detachment of the expanding droplet cannot hold against

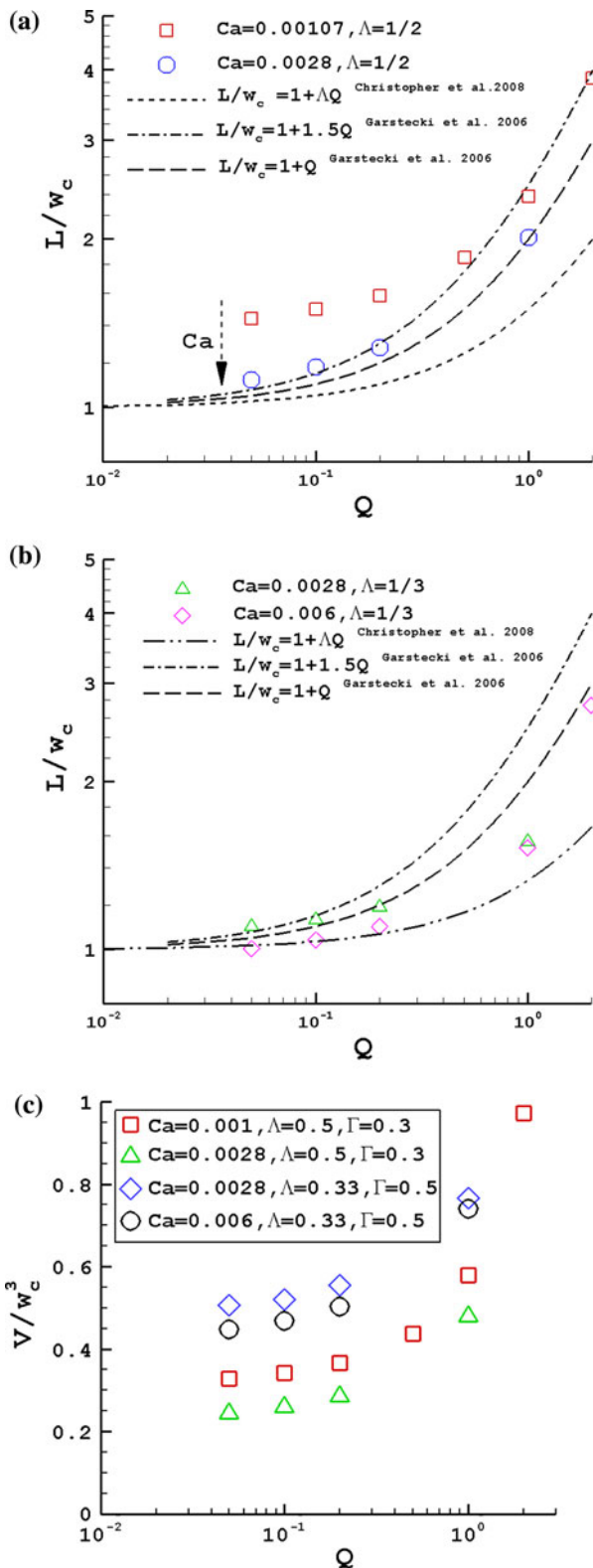


Fig. 9 a, b Non-dimensional length of drops formed versus flow rate ratio for Capillary numbers in the squeezing regime for two different geometries; c normalized droplet volume as a function of

the sum of the viscous drag due to the continuous phase flow and the pressure force due to the blockage of the passage for the continuous phase. From this force balance, one can write the non-dimensional length of the droplets

$$\bar{L} = \bar{b} + \frac{\Lambda}{\bar{b}}Q \tag{23}$$

where \bar{b} is the dimensionless length of the emerging droplet, and satisfies the following equation

$$(1 - \bar{b})^3 = \bar{b}Ca \tag{24}$$

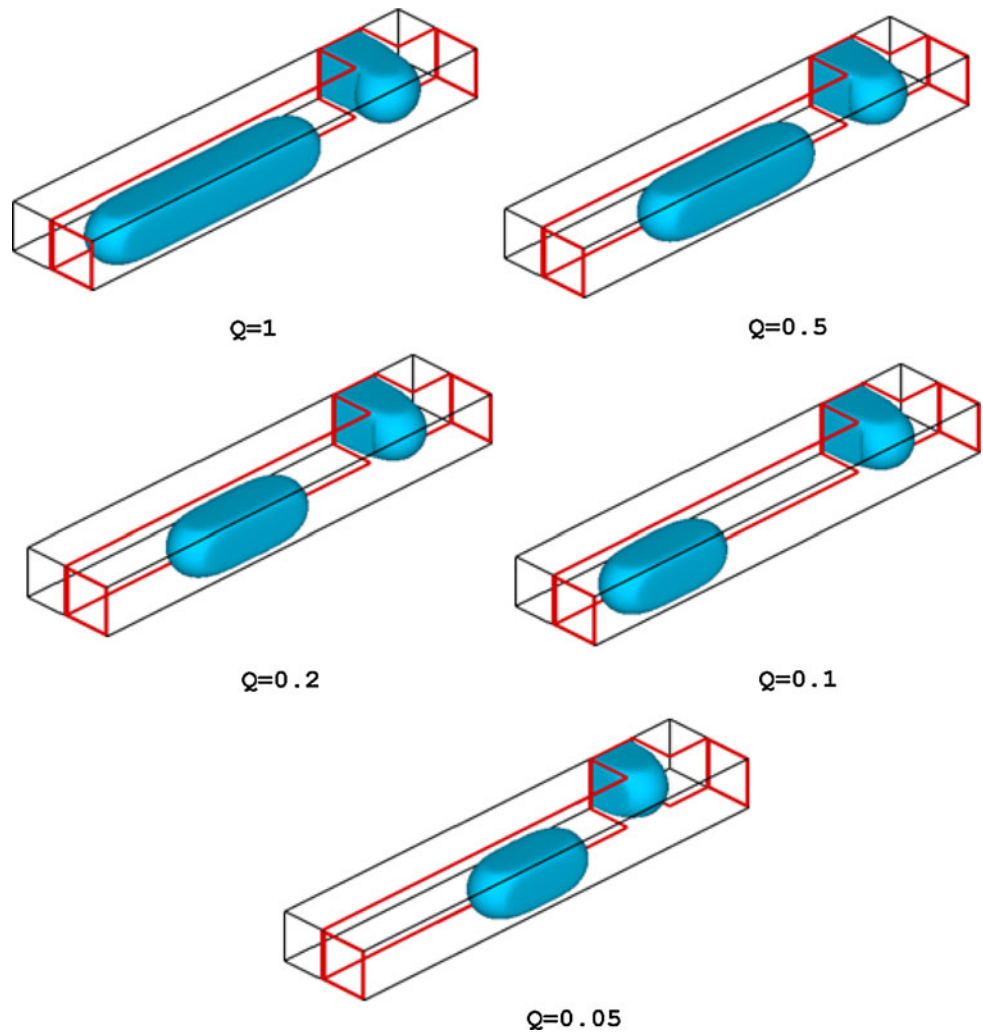
A comparison of the experimental data (Christopher et al. 2008) with Eq. 23 for the flow rate range given by 0.01-10 was found to be in reasonable agreement, although due to an approximate form of the forces and simplistic assumptions that have been made to predict the dynamics of droplet formation, discrepancies can arise when comparing other experimental data with this model.

For the sake of comparison of current simulation results with the experimental data, the droplet lengths as predicted by Eq. 24 for $\bar{b} \approx 1$, and those predicted by Eq. 21 are shown by dotted lines in Fig. 9 for the different sets of geometries simulated. Although the numerical results predict droplet lengths to be linearly proportional to the flow rate ratio and are of the same order as those predicted by the data fitted Eqs. 21 and 24, these analyses do not take into account the Capillary number effect on the size of the droplets formed. Current results indicate that the droplet length decreases as Ca increases for a fixed Q for both Λ values. The geometry-independent correlations proposed by Garstecki et al. (2006) and Christopher et al. (2008) appear to do well when the Capillary number is very low or when the flow rate ratio is less than 0.5. This was also seen in Figs. 7, 8 for flow rate ratios, $Q < 0.2$ for which the droplets were shaped like constant diameter cobbles. As the Capillary number is decreased to $Ca = 0.00107$ (Fig. 9a), the discrepancy seen with the current data and the correlations is significant even for small flow rate ratios. Christopher et al. (2008) had also observed that droplet lengths decrease with an increase in the Capillary number, and Eq. 24 under-predicted the length measured in experiments for a range of flow parameters, as it does when compared with the current LBM results.

3.2 Effect of channel depth

Having compared the current results with empirical correlations, the role of the channel depth (on the length and shapes of the droplets) is now examined. Theoretical study on establishing the role of viscosity on the size of droplets formed in the squeezing regime has been carried out (De Menech et al. 2008), but the role of geometry has not

Fig. 10 Formation of plugs as a function of flow rate ratio for $Ca = 0.001, Re_c = 0.2, \Lambda = 1, \Gamma = 1,$ and $\lambda = 1/10$



been investigated by any group to the best of our knowledge. In the current simulations, in order to understand the influence of the channel depth and to reduce the dependence on other parameters, the widths of the continuous and dispersed phase channels are kept fixed at $\Lambda = 1$, and the viscosity ratio is held constant at $\lambda = 1/10$ corresponding to a fixed Capillary number given by $Ca = 0.001$.

Figures 10 and 11 show the results for $\Gamma = 1$ and 0.5, respectively, for a range of flow rate ratios, with $201 \times 41 \times 21$ and $201 \times 41 \times 11$ nodes, respectively. The shape of the droplets formed at the T-junction resembles long plugs whose length increases with increasing flow rate ratio, as seen in earlier cases. Comparing the results in Figs 10 and 11 for the two channel heights, it can be seen that the size of the plugs formed decreases as the depth of the channel is decreased. This behavior is also seen in Fig 2 which compares the plug lengths for three different Γ 's for the same flow rate ratio of 0.1. The models given by Eq 8.1 and 24 predict that for the same flow rate ratio and equal widths of the two inlet

channels, the resulting lengths of the plugs must be the same. This is contrary to the simulation results shown in Fig. 12. The possible differences in the experimental predictions (Garstecki et al 2006, Christopher et al 2008), and current simulations can be attributed to the reason that the former were based on geometries where the channel depth was less than the width of the continuous phase channel and thus may not be applicable for geometries with $\Lambda = 1$.

The dimensionless droplet lengths for different simulations are shown in Fig 13. Based on the formulation of Wu et al. (2008), the length of the plug can be considered to be a contribution of two steps: growth length and squeeze length. Hence, the length of the plug can be written as $L/w_c = \epsilon + \omega Q$ (25) where ϵ and ω are fitting parameters that are mainly dependent on the channel geometry, and varies between 0 and 5. Current simulations were found to obey the dependence given by Eq 25, with the fitting parameters (shown in Fig. 13) determined to be of order unity as well.

Fig. 11 Formation of plugs as a function of flow rate ratio for $Ca = 0.001, Re_c = 0.1, \Lambda = 1, \Gamma = 0.5,$ and $\lambda = 1/10$

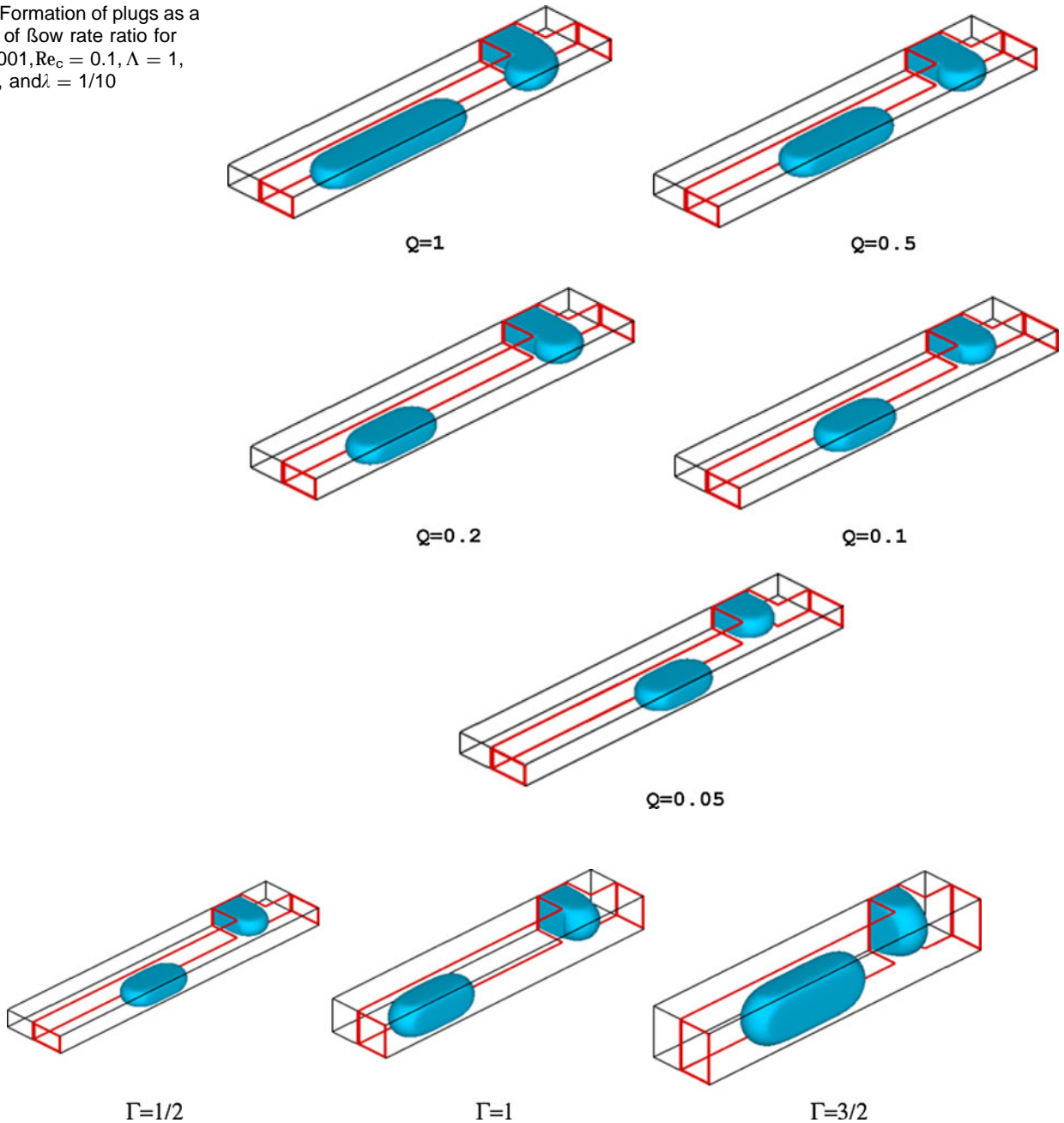


Fig. 12 Comparison of plug shapes for $Ca = 0.001$ and $\lambda = 1/10$ for different depths of the microfluidic assembly

The deviation of the simulation results from the experimental correlation given by Eq. 21 (given for $\Gamma < 4/5$) can be written as $\delta_s = \sigma h$ (if $\Gamma < 1$), or $F_\sigma = \sigma w_c$ (if $\Gamma > 1$). Consequently, for a flow geometry with $h > w_c$, the upstream pressure has to overcome a higher Laplace pressure difference across the interface of the two fluids to push the protruding droplet against the downstream edge of the dispersed phase. Understandably, $t_{growth}^{\Gamma=0.5} < t_{growth}^{\Gamma=1.0} < t_{growth}^{\Gamma=1.5}$ for the same width w_c . Once the protruding droplet blocks the main channel, the pressure build-up begins at the upstream edge. This upstream pressure surpasses the stabilizing force of the interface, and the droplet is pinched off. In the current simulations, the time taken for

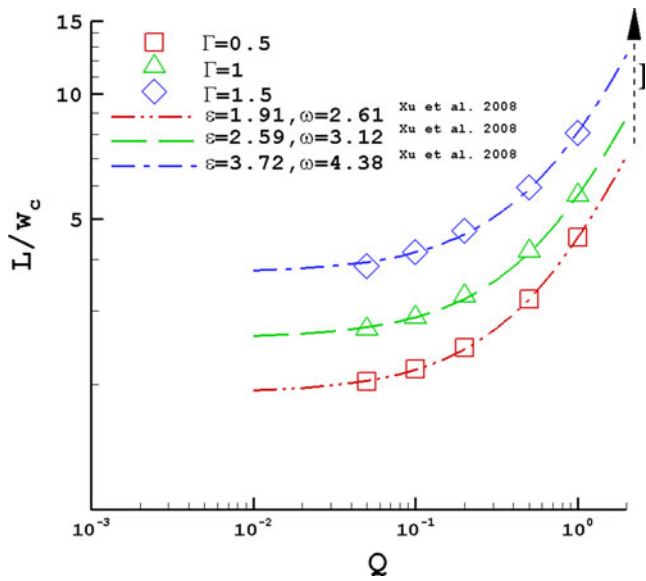


Fig. 13 Non-dimensional length of drops formed versus flow rate ratio for $Ca = 0.001$ and different depths of the T-junction device. Symbols represent the simulation results. Dotted lines, fitted to the simulation results, represent the function $L/w_c = \epsilon + \omega Q$ (Wu et al. 2008)

the pinch-off of droplets increases with an increase in the depth of the channel, an observation consistent with the pressure build-up analysis. This longer time duration for the complete detachment of the droplet explains the increase in size of the plugs for an increase in the depth of the channel observed in the current simulations.

4 Conclusions

In this study, flow regimes obtained as a consequence of two immiscible fluids interacting at a T-junction for very low Capillary numbers and different flow rates of the continuous and dispersed phases have been presented. Droplet formation in this regime was shown to be governed by the build-up of pressure on the upstream side of the protruding dispersed phase as the constriction for the passage of the continuous fluid keeps getting smaller. Three-dimensional lattice Boltzmann-based simulations in the T-junction device indicate that the length of the plugs increases linearly with an increase in the flow rate ratio for a constant Capillary number, an observation consistent with experimental data (Garstecki et al. 2006; Christopher et al. 2008; Xu et al. 2008). In addition, as the Capillary number increases, the length of the plugs was observed to decrease for a fixed flow rate ratio. The influence of the channel depth was also investigated. An increase in the depth resulted in an increase in the size of the plugs for fixed Capillary number and flow rate ratio, an observation consistent with the force mechanics at the two-fluid

interface. Empirical models, although found to capture the size of the plugs for a range of flow rate ratios, were found to be inadequate when Ca is low, or the flow rate ratio is high. A phenomenological model that could be used universally for a range of flow conditions and geometries of the T-junction device is required.

References

Anna SL, Bontoux N, Stone HA (2003) Formation of dispersions using flow focusing in microchannels. *Appl Phys Lett* 82(3):364-366

Chen S, Doolen GD (1998) Lattice Boltzmann method for fluid flows. *Ann Rev Fluid Mech* 30:329-364

Christopher GF, Anna SL (2007) Microfluidic methods for generating droplet streams. *J Phys D* 40:R319-R336

Christopher GF, Noharuddin NN, Taylor JA, Anna SL (2008) Experimental observations of the squeezing-to-dripping transition in T-shaped microfluidic junctions. *Phys Rev E* 78:036317

Cramer C, Fischer P, Windhab EJ (2004) Drop formation in a co-flowing ambient fluid. *Chem Eng Sci* 59:3045-3058

De Menech M, Garstecki P, Jousse F, Stone HA (2008) Transition from squeezing to dripping in a microfluidic T-shaped junction. *J Fluid Mech* 595:141-161

Garstecki P, Stone HA, Whitesides GM (2005) Mechanism for flow-rate controlled breakup in confined geometries: a route to monodisperse emulsions. *Phys Rev Lett* 94:164501

Garstecki P, Fuerstman MJ, Stone HA, Whitesides GM (2006) Formation of droplets and bubbles in a microfluidic T-junction: scaling and mechanism of break-up. *Lab Chip* 6:437-446

Gu X, Gupta A, Kumar R (2009) Lattice Boltzmann simulation of surface impingement at high density ratio. *J Thermophys Heat Trans* (in print)

Guillot P, Colin A (2005) Stability of parallel flows in a microchannel after a T-junction. *Phys Rev E* 72:066301

Gunstensen AK, Rothman DH, Zaleski S, Zanetti G (1991) Lattice Boltzmann model of immiscible fluids. *Phys Rev A* 43:4320-4327

Gupta A, Kumar R (2008) Lattice Boltzmann simulation to study multiple bubble dynamics. *Int J Heat Mass Transf* 51:5192-5203

Gupta A, Murshed SMS, Kumar R (2009) Droplet formation and stability of flows in a microfluidic T-junction. *Appl Phys Lett* 94:161407

Husny J, Cooper-White JJ (2006) The effect of elasticity on drop creation in T-shaped microchannels. *J Non-Newton Fluid Mech* 137:121-136

Inamura T, Tajima S, Ogino F (2004) Lattice Boltzmann simulation of droplet collision dynamics. *Int J Heat Mass Transf* 47:4649-4657

Latva-Kokko M, Rothman DH (2005) Diffusion properties of gradient-based lattice Boltzmann models of immiscible fluids. *Phys Rev E* 71:056702

Lishchuk SV, Care CM, Halliday I (2003) Lattice Boltzmann algorithm for surface tension with greatly reduced microcurrents. *Phys Rev E* 67:036701

Lishchuk SV, Halliday I, Care CM (2008) Multicomponent lattice Boltzmann method for fluids with a density contrast. *Phys Rev E* 77:036702

Shan X, Chen H (1993) Lattice Boltzmann model for simulating flows with multiple phases and components. *Phys Rev E* 47:1815-1819

- Swift M, Osborne W, Yeomans J (1995) Lattice Boltzmann simulation of nonideal fluids. *Phys Rev Lett* 75:830–833
- Thorsen T, Roberts RW, Arnold FH, Quake SR (2001) Dynamic pattern formation in a vesicle-generating microfluidic device. *Phys Rev Lett* 86(18):4163–4166
- Tice JD, Lyon AD, Ismagilov RF (2004) Effects of viscosity on droplet formation and mixing in microfluidic channels. *Anal Chim Acta* 507:73–77
- Umbanhowar PB, Prasad V, Weitz DA (2000) Monodisperse emulsion generation via drop break off in a co-flowing stream. *Langmuir* 16:347–351
- Van der Graaf S, Nisisako T, Schroeder CGPH, van der Sman RGM, Boom RM (2006) Lattice Boltzmann simulations of droplet formation in a T-shaped microchannel. *Langmuir* 22:4144–4152
- Wu L, Tsutahara M, Kim LS, Ha MY (2008) Three-dimensional lattice Boltzmann simulations of droplet formation in a cross-junction microchannel. *Int J Multiph Flow* 34:852–864
- Xu JH, Li SW, Tan J, Luo GS (2008) Correlations of droplet formation in T-junction microfluidic devices: from squeezing to dripping. *Microfluid Nanofluid* 5:711–717